

Hadronic vacuum polarization with C* boundary conditions

Anian Altherr,^{a,*} Roman Gruber,^{a,*} Lucius Bushnaq,^b Isabel Campos,^c Marco Catillo,^a Alessandro Cotellicci,^d Madeleine Dale,^{d,e,f,g} Patrick Fritzsche,^b Javad Komijani,^a Jens Lücke,^{d,h} Marina Krstić Marinković,^a Sofie Martins,ⁱ Agostino Patella,^{d,h} Nazario Tantalo^{e,f} and Paola Tavella^a

^a*Institut für Theoretische Physik, ETH Zürich, Zürich, Switzerland*

^b*School of Mathematics, Trinity College Dublin, Dublin, Ireland*

^c*Instituto de Física de Cantabria & IFCA-CSIC, Santander, Spain*

^d*Institut für Physik & IRIS Adlershof, Humboldt Universität zu Berlin, Berlin, Germany*

^e*Università degli Studi di Roma "Tor Vergata", Rome, Italy*

^f*INFN, Sezione di Tor Vergata, Rome, Italy*

^g*Department of Physics, University of Cyprus, Nicosia, Cyprus*

^h*DESY, Zeuthen, Germany*

ⁱ*University of Southern Denmark, Odense, Denmark*

E-mail: aaltherr@ethz.ch, rgruber@ethz.ch

We present a progress report on the calculation of the connected hadronic contribution to the muon $g - 2$ with C* boundary conditions. For that purpose we use a QCD gauge ensemble with 3+1 flavors and two QCD+QED gauge ensembles with 1+2+1 flavors of dynamical quarks generated by the RC* collaboration. We detail the calculation of the vector mass and elaborate on both statistical and systematic errors.

*The 39th International Symposium on Lattice Field Theory,
8th-13th August, 2022,
Rheinische Friedrich-Wilhelms-Universität Bonn, Bonn, Germany*

*Speaker

1. Introduction

There has been a tantalizing discrepancy between the experimental and theoretical values for the anomalous magnetic moment of the muon [1]. On the experimental side, two experiments at Fermilab [2] and J-PARC [3] are aiming to further decrease the uncertainty in the next few years. Hence, progress on the theoretical side is crucial to keep up with experiments. The main uncertainty in the theoretical calculation stems from the hadronic vacuum polarization (HVP) contribution. To keep up with experimental precision, a subpercent precision is required for the HVP contribution. While there exist several sub-percent calculations of the connected light contribution (see Ref. [1] for an overview) at the isospin-symmetric point, the systematic uncertainty due to neglecting isospin-breaking effects becomes crucial. Several collaborations have started to take these effects into account for the anomalous magnetic moment [4–10].

There exist different ways of including these effects; for a detailed review of some of these methods see Ref. [11, 12]. Among these is QED_L that removes the zero modes of the photonic field by hand [13] and thus creates a non-local field theory. Alternatively, QED_m uses a finite photon mass as an infrared regulator [14, 15], but requires an extrapolation to zero photon mass. In QED_∞ the QED part is analytically calculated in the continuum [16–18]. In this proceedings, we choose QED_C in which the zero modes of the photon field are absent due to C^* boundary conditions [19–24], thus allowing for a local field theory without including an additional regulator. Using these boundary conditions, we explore the connected HVP contribution.

After a brief introduction to the HVP in Section 2, we introduce a few aspects of C^* boundary conditions in Section 3. In Section 4 we present our results of vector masses and the HVP and conclude in Section 5.

2. Hadronic vacuum polarization

The HVP to the muon anomalous magnetic moment can be obtained using the time-momentum representation [25]:

$$a_\mu^{\text{HVP}} = \left(\frac{\alpha}{\pi}\right)^2 \int_0^\infty dx_0 G(x_0) \tilde{K}(x_0; m_\mu). \quad (1)$$

Here α is the electromagnetic coupling, $\tilde{K}(x_0; m_\mu)$ is a kernel function defined in Ref. [26, Eq. (8)] with the muon mass m_μ , and $G(x_0)$ is expressed in terms of the two-point correlation function of the electromagnetic current $j_k(x)$:

$$G(x_0) = -\frac{1}{3} \sum_{k=1}^3 \int d^3x \langle j_k(x) j_k(0) \rangle. \quad (2)$$

The integral over time x_0 in Eq. (1) can be split into two parts to take into account the finite-time extent on the lattice and to treat the noise that dominates the signal for large times separately [25], see Section 4.2.

3. C^* boundary conditions

At the target precision of one percent it is crucial to include QED effects in lattice simulations, as they are expected to be of the order of one percent. A naive implementation of QED on a finite-volume lattice with periodic boundary conditions does not allow to simulate charged particles because states with non-zero electric charge violate Gauss' law. C^* boundary conditions [19–23] provide a remedy, and they do not lead to a non-local field theory as opposed to QED_L . The fields obey the following constraints in spatial direction $\hat{k} = \hat{1}, \hat{2}, \hat{3}$

$$\begin{aligned}\psi_f(x + L\hat{k}) &= \psi_f^c(x) := C^{-1}\bar{\psi}_f^T(x) \\ \bar{\psi}_f(x + L\hat{k}) &= \bar{\psi}_f^c(x) := -\psi_f^T(x)C \\ U_\mu(x + L\hat{k}) &= U_\mu^c(x) := U_\mu(x)^* \\ A_\mu(x + L\hat{k}) &= A_\mu^c(x) := -A_\mu(x),\end{aligned}\tag{3}$$

where ψ_f and $\bar{\psi}_f$ are the fermionic fields of flavor f , $U_\mu(x) \in SU(3)$ are the QCD gauge links and $e^{iA_\mu(x)} \in U(1)$ are the QED gauge links; U_μ^* denotes complex conjugation and we denote charge conjugation by the superscript c . The charge conjugation matrix C obeys $C\gamma_\mu C^{-1} = -\gamma_\mu^T$ with the Euclidean gamma matrices γ_μ . We note that the photon field $A_\mu(x)$ is antiperiodic and thus does not have a zero-momentum component by construction.

3.1 Correlation functions

It is useful to combine ψ_f and $\bar{\psi}_f$ into a spinor doublet

$$\chi_f(x) = \begin{pmatrix} \psi_f(x) \\ \psi_f^c(x) \end{pmatrix}\tag{4}$$

and express the action in terms of χ_f . When using the Wilson-Dirac formulation with a Sheikholeslami-Wohlert improvement term (see Refs. [27, 28] for details), we find that the fermionic action can be written as

$$S = -\frac{1}{2} \sum_{f=1}^{N_f} \chi_f^T C \sigma_1 D \chi_f,\tag{5}$$

where σ_1 is the first Pauli matrix acting on the spinor doublet in Eq. (4) and N_f is the number of flavors. We note that D has $24V \times 24V$ complex components as it acts on a spinor doublet (V denotes the lattice volume). Wick contractions yield (see Ref. [23, Appendix B])

$$\overline{\chi_f(x) \chi_{f'}(y)}^T = -\delta_{f,f'} D_{f'}^{-1}(x; y) \sigma_1 C^{-1}.\tag{6}$$

To evaluate the two-point function in Eq. (1) we use

$$j_\mu(x) = \frac{1}{2} \sum_{f=1}^{N_f} q_f \chi_f^T(x) \sigma_3 \sigma_1 C \gamma_\mu \chi_f(x),\tag{7}$$

where q_f the charge of flavor f , σ_3 the third Pauli matrix acting on the spinor doublet. When expressed in terms of ψ_f and $\bar{\psi}_f$, $j_\mu(x)$ is equivalent to the familiar expression $\sum_f q_f \bar{\psi}_f(x) \gamma_\mu \psi_f(x)$. Inserting Eq. (7) into the two-point correlation function, we find

$$\langle j_\mu(x) j_\nu(y) \rangle = \langle j_\mu(x) j_\nu(y) \rangle_{\text{conn}} + \langle j_\mu(x) j_\nu(y) \rangle_{\text{disc}},$$

where in this proceedings we only take the connected contractions into account¹:

$$\langle j_\mu(x) j_\nu(y) \rangle_{\text{conn}} = \frac{1}{2} \sum_{f=1}^{N_f} q_f^2 \text{tr} \left[\sigma_3 D_f^{-1}(x; y) \gamma_\nu \sigma_3 D_f^{-1}(y; x) \gamma_\mu \right], \quad (8)$$

and neglect the disconnected contribution

$$\langle j_\mu(x) j_\nu(y) \rangle_{\text{disc}} = \left(\frac{1}{2} \sum_{f=1}^{N_f} q_f \text{tr} \left[\sigma_3 \gamma_\mu D_f^{-1}(x; x) \right] \right) \left(\frac{1}{2} \sum_{f=1}^{N_f} q_f \text{tr} \left[\sigma_3 \gamma_\nu D_f^{-1}(y; y) \right] \right). \quad (9)$$

This expression is similar to the one obtained in periodic boundary conditions, the only difference being that D^{-1} has $24V \times 24V$ components.

3.2 Lattice parameters

We use configurations generated by the RC^{*} collaboration [29] with 3+1 and 1+2+1 flavors of Wilson quarks with a clover term for both $SU(3)$ and $U(1)$. The $SU(3)$ action is $O(a)$ -improved in a non-perturbative way for QCD ensembles [30], which is valid for QCD+QED ensembles up to $O(\alpha)$, and the $U(1)$ action is (so far) tree-level improved. All configurations use C^* boundary conditions (see Section 3) and are summarized in Table 1. There is one QCD ensemble (A400a00b324) and two ensembles with dynamically generated QCD+QED fields (A360a50b324 and A380a07b324) at two values of the fine structure constant; one is close to the physical value and one is larger. The charged pion mass ranges between approximately 360 MeV and 400 MeV and we have $m_{\pi^\pm} L \approx 2.9 - 3.5$. We use the reference value $\sqrt{8t_0} = 0.415$ fm [31] to obtain physical units. We refer to Ref. [29] for the details of the generation.

4. Preliminary results

In this section, we first examine the signal-to-noise ratio of the two-point function and then show values for the vector masses and the HVP. Our analysis is based on the openQ*D program package [32].

4.1 Signal-to-noise

Using the three ensembles in Table 1 we calculate the two-point function in time-momentum representation $G(x_0)$. As illustrated in Figure 1, the relative statistical error for simulating QCD (A400a00b324) is comparable to the error of simulating QCD+QED at physical α (A380a07b324). On the other hand, simulating QCD+QED at unphysically large α (A360a50b324) yields larger errors than for physical α . This might be due to a lower pion mass (360 MeV for A360a50b324) compared to the other ensembles.

¹We note that there are two combinations of Wick contractions that contribute to the connected part.

ensemble	A360a50b324	A380a07b324	A400a00b324
flavors	1 + 2 + 1	1 + 2 + 1	3 + 1
β	3.24	3.24	3.24
α_R	0.040633(80)	0.007081(19)	0.0
m_{π^\pm} [MeV]	358.6(3.7)	383.6(4.4)	398.5(4.7)
a [fm]	0.05054(27)	0.05323(28)	0.05393(24)
number of used configurations	181	200	200

Table 1: Summary of used ensembles and their parameters, compare Ref. [29] for details. All lattices have size $32^3 \times 64$. Ensembles with 1+2+1 flavor decomposition have degenerate down and strange quark, ensembles with 3+1 flavor decomposition have degenerate up, down and strange quark. The name of the ensemble — say A360a50b324 — contains the approximate charged pion mass (360 MeV), the bare fine-structure constant (0.050) and the coupling (3.24). We denote the renormalized fine-structure constant by α_R and also tabulate the number of used configurations. Note that we have not used all available configurations, which is about 2000 for each ensemble. We use the reference value $\sqrt{8t_0} = 0.415$ fm [31] to obtain physical units.

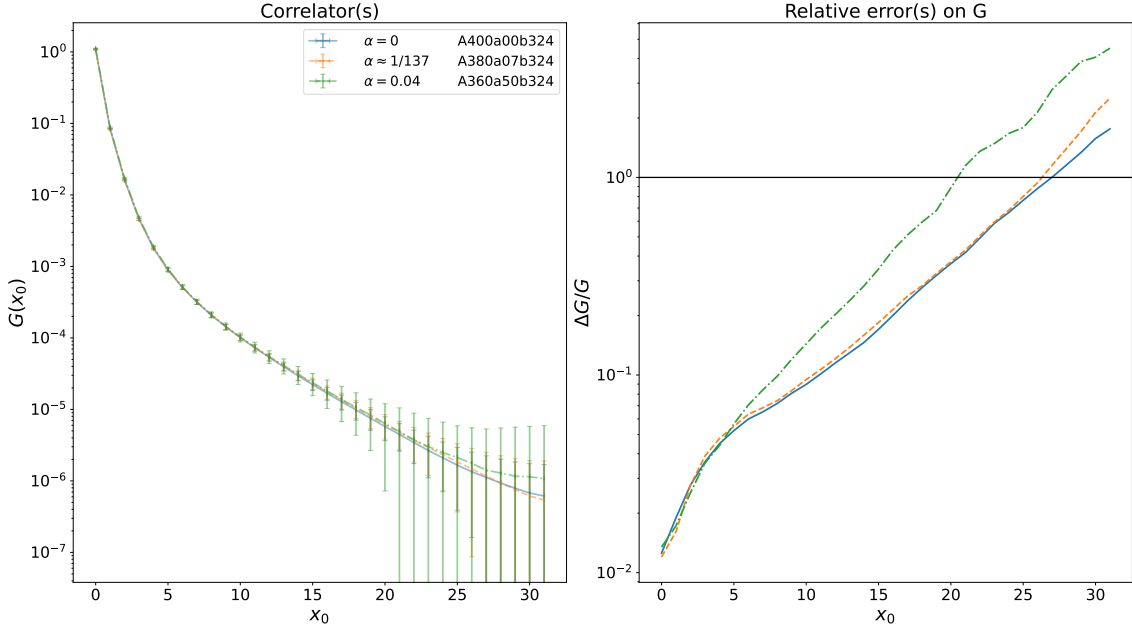


Figure 1: Relative error comparison. On the left-hand side, we plot the local-local two-point function of the electromagnetic current $G(x_0)$, on the right-hand side we plot the relative errors. The errors for the QCD ensemble (blue solid line) and the QCD+QED ensemble with physical α have comparable relative errors, whereas the relative error for the QCD+QED ensemble with larger α is slightly larger. The number of used gauge configurations and stochastic sources are 181 and 10, respectively in all three cases.

ensemble	quark	m_{eff}	χ_r^2
A360a50b324	down/strange	0.262(7)	1.03
	up	0.267(8)	0.93
A380a07b324	down/strange	0.265(6)	1.07
	up	0.266(4)	0.95
A400a00b324	up/down/strange	0.278(7)	0.94

Table 2: Vector meson mass for the three ensembles: The effective mass m_{eff} is obtained by performing a χ^2 -fit of the two-point function Eq. (2) to a single exponential Eq. (10). In the last column, we display the χ^2 value per degree of freedom χ_r^2 .

4.2 Mass spectroscopy

As the signal-to-noise ratio deteriorates for large times x_0 , we introduce a $x_{0,\text{cut}}$ and replace the two-point function $G(x_0)$ by a model function for $x_0 > x_{0,\text{cut}}$. In finite volume the two-point function $G(x_0)$ can be written as a sum of exponentials with positive coefficients. We choose to only consider the leading term in the spectral decomposition for our model function

$$G(x_0)_{\text{model}} = Ae^{-m_{\text{eff}}x_0}, \quad (10)$$

where m_{eff} is the effective mass of the corresponding vector meson ground state in lattice units and A the decay amplitude.

In order to determine the coefficients m_{eff} and A , we perform a χ^2 -fit to the two-point correlation function in a fit range I_{fit} where excited states have decayed sufficiently, but where there is still a clear signal. Since we are interested in the ground state, we apply Gaussian smearing to the sink and source point to increase the overlap with the ground state. In addition, we apply stout smearing to the gauge fields. The effective mass m_{eff} is then extracted by using a 1-parameter logarithmic fit to the correlator on a subset of 40 configurations. Finally, we use the effective mass as input for the 1-parameter fit of the decay amplitude to the two-point function (obtained with point sources, without smearing). In the future we plan to improve the model function by including excited states.

Table 2 shows a compilation of the extracted masses. The statistical error is obtained using the jackknife method and the systematic error due to choosing a fit range for the vector mass is estimated by varying the range I_{fit} . The total error in the table equals the two error contributions added in quadrature. The mass of the ground state for the charm contribution is not determined because the model part of the correlator has a negligible contribution to the HVP in that case (see Figure 2).

4.3 Hadronic vacuum polarization contribution

As a preliminary check we plot the integrand of Eq. (1) in Figure 2. Here we use a combination of conserved and local currents, i.e., $G(x_0)$ is obtained from $\langle j_k^{\text{conserved}}(x)j_k^{\text{local}}(0) \rangle$. The use of local currents simplifies the calculations, but requires both a multiplicative as well as an additive renormalization constant [33]. We set the renormalization constant due to the local current to unity. The results for the HVP contribution of muon $g - 2$ are shown in Table 3.

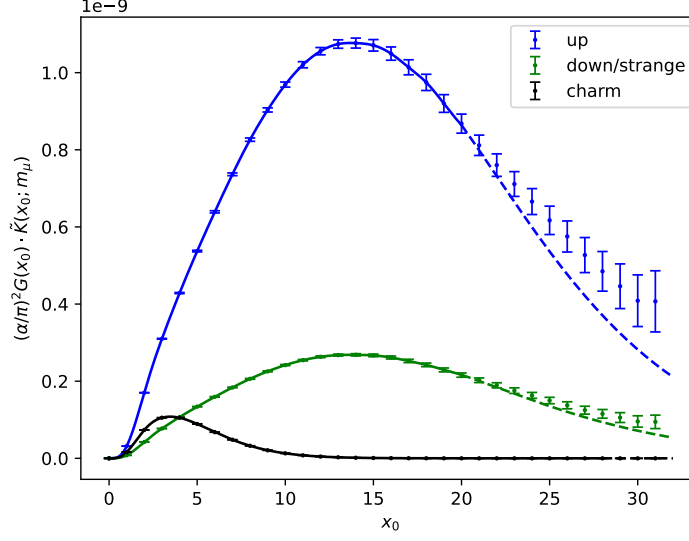


Figure 2: Integrand of the HVP contribution for the A380a07b324 ensemble where we use a conserved-local two-point function. Points label the actual lattice data, solid lines symbolize interpolation (for $x_0 < x_{0,\text{cut}}$) and dashed lines stand for the model function ($x_0 \geq x_{0,\text{cut}}$) respectively. The systematic error occurring due to using only a single exponential for the model part is significant for the up contribution (blue) and down/strange contribution (green); for the charm contribution (black) it is negligible.

ensemble	flavor	$a_\mu^{\text{HVP}} \times 10^{10}$
A360a50b324	up	309(11)
	down/strange	77(2)
	charm	10.62(11)
A380a07b324	up	331(7)
	down/strange	83(2)
	charm	9.78(10)
A400a00b324	up/down/strange	319(8)
	charm	9.97(9)

Table 3: Results for the HVP contribution. The ensembles employ C^* boundary conditions in spatial directions, have a pion mass of approximately 360, 380, and 400 MeV respectively, and are simulated on a lattice with extent $32^3 \times 64$ (compare Table 1). We use a combination of conserved and local current and set the renormalization constant to unity.

4.4 Error contributions

We display the error contributions for the up-quark contribution of the QCD+QED ensemble with physical α in Table 4. An estimate of the statistical Monte Carlo error is obtained using jackknife. The error occurring in the determination of the vector mass (compare Table 2) affects the precision of the HVP contribution as does the error on the lattice spacing. The lattice spacing has been determined in Ref. [29], which is based on the value of the the gradient flow scale t_0 determined in Ref. [31]; the relative error of the lattice spacing turns out to be $\frac{\Delta a}{a} = 0.53\%$ (see

	variation w.r.t.	relative error
statistical	jackknife	1.21%
	err. prop. of vector mass	1.36%
	err. prop. of scale setting	0.92%
systematic	fit range	0.14%
	model cutoff $x_{0,\text{cut}}$	0.03%
	excited states	1.20%
total		2.37%

Table 4: Error contributions of the up contribution for ensemble A380a007b324. The row ‘jackknife’ quantifies the error due to statistical fluctuations in the Monte Carlo simulation. The second row quantifies the error propagation of the uncertainty on the vector mass (see Section 4.2) and the third row the error propagation of the uncertainty on the lattice spacing. The error due to selecting a fit range (for the vector mass and the amplitude), and a model cutoff $x_{0,\text{cut}}$ are quantified by varying these parameters, the error due to neglecting excited states is estimated by using a bounding method. We do not assess continuum extrapolation nor chiral extrapolation, neither do we estimate finite-size effects.

Table 1). We note that the gradient flow scale has only been determined for QCD ensembles, a scale setting in full QCD+QED remains to be worked out; see Ref. [12]. The contribution to the uncertainty on the HVP due to error propagation of the uncertainty in scale setting is expected to be roughly $1.8 \frac{\Delta a}{a}$ (see Ref. [26, Appendix B.2]), which agrees with our findings. In addition to statistical errors, we have systematic errors. Due to the exploratory nature of this proceedings we do not carry out a continuum extrapolation nor a chiral extrapolation to physical meson masses. Neither do we assess finite-size effects. There are further systematic errors due to the model part. To determine the vector mass and amplitude in Eq. (10) we select a fit range and a cutoff $x_{0,\text{cut}}$. We estimate the error due to that choice by varying the cutoff and the fit range around our chosen value. These errors are small compared to the error that arises due to neglecting excited states. We estimate the contribution of excited states by bounding the correlator from above and estimating the error as the difference between the bounds [4]. In the future we plan to reduce the error contributions individually, see Section 5.

5. Conclusion and outlook

We have presented the first calculation of the connected HVP contribution to the muon $g - 2$ using C^* boundary conditions. Three different ensembles are used, a QCD ensemble and two QCD+QED ensembles with different values of the fine structure constant. The noise level for the ensemble with physical α is comparable to the ensemble with QCD only, whereas for larger α the noise level increases. There remain a couple of open questions that we plan to address in the future.

First, isospin-breaking effects have not been addressed in the QCD ensemble A400a00b324. There are two methods to deal with isospin-breaking effects — a perturbative or a stochastic approach. In the perturbative approach, we expand the QCD+QED action around the isospin-symmetric point ($\alpha = 0$, $m_u - m_d = 0$) in α and $m_u - m_d$ and evaluate the correlation function obtained in that way [34, 35]. On the other hand, QED fields can be added stochastically by

multiplying QCD gauge links with random $U(1)$ -phases [35, 36]. We plan to investigate both approaches.

Second, finite-size effects for the HVP can be quantified using the Hansen-Patella method [37], where different orders of finite-volume effects are generated by powers of $e^{-m_\pi L}$ with m_π the pion mass, and L the linear lattice extent. For periodic boundary conditions the leading-order term is $\mathcal{O}(e^{-m_\pi L})$ whereas for C^* boundary conditions this leading order vanishes and finite-size effects are of the order $\mathcal{O}(e^{-\sqrt{2}m_\pi L})$ [38]. In addition, there are power-law finite-size effects due to QED, which are expected to be smaller compared to periodic boundary conditions (see for example Refs. [22] for corrections to baryon masses).

Third, as seen in Table 4, we need to implement additional variance-reduction methods to achieve a sub-percent precision. Firstly, we plan to increase the number of configurations and number of sources to decrease the statistical error and to increase the precision of the vector mass determination. In addition, low-mode averaging [39, 40] exploits the structure of the Dirac operator and reduces the variance that stems from the low modes. Regarding ensemble generation, multi-level Monte Carlo [41] reduces the variance in the correlators exponentially in the distance. We plan to consider more sophisticated model functions than single exponentials; this will further decrease the error due to the model part.

Acknowledgments

We acknowledge access to Piz Daint at the Swiss National Supercomputing Centre, Switzerland under the ETHZ's share with the project IDs s1101, eth8 and go22. AA's and RG's research is funded by Schweizerischer Nationalfonds Project No. 200021_200866. SM received funding from the European Union's Horizon 2020 research and innovation programme under the Marie Skłodowska-Curie grant agreement № 813942. AC's and JL's research is funded by the Deutsche Forschungsgemeinschaft Project No. 417533893/GRK-2575 "Rethinking Quantum Field Theory".

References

- [1] T. Aoyama, N. Asmussen, M. Benayoun, J. Bijnens, T. Blum, M. Bruno et al., *The anomalous magnetic moment of the muon in the Standard Model*, *Physics Reports* **887** (2020) 1 [2006.04822].
- [2] MUON $g - 2$ COLLABORATION collaboration, *Measurement of the positive muon anomalous magnetic moment to 0.46 ppm*, *Phys. Rev. Lett.* **126** (2021) 141801.
- [3] M. Abe, S. Bae, G. Beer, G. Bunce, H. Choi, S. Choi et al., *A new approach for measuring the muon anomalous magnetic moment and electric dipole moment*, *Progress of Theoretical and Experimental Physics* **2019** (2019) [1901.03047].
- [4] S. Borsanyi, Z. Fodor, J.N. Guenther, C. Hoelbling, S.D. Katz, L. Lellouch et al., *Leading hadronic contribution to the muon magnetic moment from lattice QCD*, *Nature* **593** (2021) 51 [2002.12347].

- [5] ETM collaboration, *Electromagnetic and strong isospin-breaking corrections to the muon $g - 2$ from lattice QCD + QED*, *Phys. Rev. D* **99** (2019) 114502.
- [6] FERMILAB LATTICE, HPQCD, AND MILC collaboration, *Strong-Isospin-Breaking Correction to the Muon Anomalous Magnetic Moment from Lattice QCD at the Physical Point*, *Phys. Rev. Lett.* **120** (2018) 152001.
- [7] FERMILAB LATTICE, HPQCD, AND MILC COLLABORATIONS collaboration, *Hadronic-vacuum-polarization contribution to the muon's anomalous magnetic moment from four-flavor lattice QCD*, *Phys. Rev. D* **101** (2020) 034512.
- [8] RBC AND UKQCD collaboration, *Calculation of the Hadronic Vacuum Polarization Contribution to the Muon Anomalous Magnetic Moment*, *Phys. Rev. Lett.* **121** (2018) 022003.
- [9] C. Lehner and A.S. Meyer, *Consistency of hadronic vacuum polarization between lattice qcd and the r ratio*, *Phys. Rev. D* **101** (2020) 074515.
- [10] A. Risch and H. Wittig, *Leading isospin breaking effects in the hvp contribution to a_μ and to the running of α* , *arXiv* (2021) [2112.00878].
- [11] A. Patella, *QED corrections to hadronic observables*, *PoS LATTICE2016* (2016) [1702.03857].
- [12] N. Tantalo, "Matching lattice QC+ED to nature." Talk at Lattice 2022, indico.hiskp.uni-bonn.de/event/40/contributions/847/ (2022-11-30).
- [13] S. Uno and M. Hayakawa, *QED in Finite Volume and Finite Size Scaling Effect on Electromagnetic Properties of Hadrons*, *Progress of Theoretical Physics* **120** (2008) .
- [14] M.G. Endres, A. Shindler, B.C. Tiburzi and A. Walker-Loud, *Massive photons: an infrared regularization scheme for lattice QCD+QED*, *Phys. Rev. Lett.* **117** (2015) [1507.08916].
- [15] M. Clark, M. Della Morte, Z. Hall, B. Hörz, A. Nicholson, A. Shindler et al., *QED with massive photons for precision physics: zero modes and first result for the hadron spectrum*, *PoS LATTICE2021* (2022) 281.
- [16] X. Feng and L. Jin, *QED self-energies from lattice QCD without power-law finite-volume errors*, *Phys. Rev. D* **100** (2019) 094509.
- [17] N.H. Christ, X. Feng, L.-C. Jin and C.T. Sachrajda, *Finite-volume effects in long-distance processes with massless leptonic propagators*, *Phys. Rev. D* **103** (2021) 014507.
- [18] T. Blum, N. Christ, M. Hayakawa, T. Izubuchi, L. Jin, C. Jung et al., *Using infinite-volume, continuum QED and lattice QCD for the hadronic light-by-light contribution to the muon anomalous magnetic moment*, *Phys. Rev. D* **96** (2017) 034515.
- [19] A.S. Kronfeld and U.J. Wiese, *SU(N) gauge theories with C-periodic boundary conditions (I). Topological structure*, *Nuclear Physics B* **357** (1991) 521.

- [20] U.J. Wiese, *C- and G-periodic QCD at finite temperature*, *Nuclear Physics B* **375** (1992) 45.
- [21] A.S. Kronfeld and U.J. Wiese, *$SU(N)$ gauge theories with C-periodic boundary conditions (II). Small-volume dynamics*, *Nuclear Physics B* **401** (1993) 190.
- [22] B. Lucini, A. Patella, A. Ramos and N. Tantalo, *Charged hadrons in local finite-volume QED+QCD with C^* boundary conditions*, *JHEP* **02** (2016) 076 [[1509.01636](#)].
- [23] M. Hansen, B. Lucini, A. Patella and N. Tantalo, *Gauge invariant determination of charged hadron masses*, *JHEP* **2018** (2018) 146.
- [24] L. Polley, *Boundaries for $SU(3)_c \times U(1)_{el}$ lattice gauge theory with a chemical potential*, *Z. Phys. C - Particles and Fields* **59** (1993) 105.
- [25] D. Bernecker and H.B. Meyer, *Vector correlators in lattice QCD: Methods and applications*, *Eur. Phys. J. A* **47** (2011) 1.
- [26] M. Della Morte, A. Francis, V. Gülpers, G. Herdoíza, G. von Hippel, H. Horch et al., *The hadronic vacuum polarization contribution to the muon $g - 2$ from lattice QCD*, *JHEP* **2017** (2017) 20 [[1705.01775](#)].
- [27] A. Patella, “Dirac operator.” Notes for openQxD: gitlab.com/rcstar/openQxD/-/blob/master/doc/dirac.pdf (2022-11-30).
- [28] A. Patella, “ C^* boundary conditions in openQxD code.” Notes for openQxD: gitlab.com/rcstar/openQxD/-/blob/master/doc/cstar.pdf (2022-11-30).
- [29] L. Bushnaq, I. Campos, M. Catillo, A. Cotellucci, M. Dale, P. Fritzsche et al., *First results on QCD+QED with C^* boundary conditions*, *arXiv* (2022) [[2209.13183](#)].
- [30] P. Fritzsche, R. Sommer, F. Stollenwerk and U. Wolff, *Symanzik improvement with dynamical charm: a $3+1$ scheme for Wilson quarks*, *JHEP* **25** (2018) 1 [[1805.01661](#)].
- [31] M. Bruno, T. Korzec and S. Schaefer, *Setting the scale for the CLS $2+1$ flavor ensembles*, *Phys. Rev. D* **95** (2017) 074504.
- [32] I. Campos, P. Fritzsche, M. Hansen, M.K. Marinkovic, A. Patella, A. Ramos et al., *openQxD code: a versatile tool for QCD+QED simulations: RC* collaboration*, *Eur. Phys. J. C* **80** (2020) 195.
- [33] J.C. Collins, A.V. Manohar and M.B. Wise, *Renormalization of the vector current in QED*, *Phys. Rev. D* **73** (2006) 105019.
- [34] G.M.D. Divitiis, P. Dimopoulos, R. Frezzotti, V. Lubicz, G. Martinelli, R. Petronzio et al., *Isospin breaking effects due to the up-down mass difference in lattice QCD*, *JHEP* **124** (2012) 1.
- [35] P. Boyle, V. Gülpers, J. Harrison, A. Jüttner, C. Lehner, A. Portelli et al., *Isospin breaking corrections to meson masses and the hadronic vacuum polarization: a comparative study*, *JHEP* **153** (2017) 153 [[1706.05293](#)].

- [36] A. Duncan, E. Eichten and H. Thacker, *Electromagnetic Splittings and Light Quark Masses in Lattice QCD*, *Phys. Rev. Lett.* **76** (1996) 3894.
- [37] M.T. Hansen and A. Patella, *Finite-volume and thermal effects in the leading-HVP contribution to muonic $g - 2$* , *JHEP* **29** (2020) 29 [[2004.03935](#)].
- [38] S. Martins, “Finite-Size Effects of the Hadronic Vacuum Polarization Contribution to the Muon ($g - 2$) with C^* Boundary Conditions.” Talk at Lattice 2022, indico.hiskp.uni-bonn.de/event/40/contributions/844/ (2022-11-30).
- [39] T. DeGrand and S. Schaefer, *Improving meson two-point functions in lattice QCD*, *Computer Physics Communications* **159** (2004) 185.
- [40] G.S. Bali, S. Collins and A. Schäfer, *Effective noise reduction techniques for disconnected loops in Lattice QCD*, *Computer Physics Communications* **181** (2010) 1570 [[0910.3970](#)].
- [41] M. Dalla Brida, L. Giusti, T. Harris and M. Pepe, *Multi-level Monte Carlo computation of the hadronic vacuum polarization contribution to ($g - 2$)*, *Physics Letters B* **816** (2021) 136191.